JMEPEG (2008) 17:240–249
DOI: 10.1007/s11665-007-9143-y

1059-9495/$19.00

The Strain-Hardening Behavior of Partially Austenitized and the Austempered Ductile Irons with Dual Matrix Structures

Volkan Kilicli and Mehmet Erdogan

(Submitted January 20, 2007; in revised form March 31, 2007)

In the current study, an unalloyed ductile iron containing 3.50 C wt.%, 2.63 Si wt.%, 0.318 Mn wt.%, and 0.047 Mg wt.% was intercritically austenitized (partially austenitized) in two-phase regions ($\alpha + \gamma$) at different temperatures for 20 min and then was quenched into salt bath held at austempering temperature of 365 °C for various times to obtain different ausferrite plus proeutectoid ferrite volume fractions. Fine and coarse dual matrix structures (DMS) were obtained from two different starting conditions. Some specimens were also conventionally austempered from 900 °C for comparison. The results showed that a structure having proeutectoid ferrite plus ausferrite (bainitic ferrite + high-carbon austenite (retained or stabilized austenite)) has been developed. Both of the specimens with ~75% ausferrite volume fraction (coarse structure) and the specimen with ~82% ausferrite volume fraction (fine structure) exhibited the best combination of high strength and ductility compared to the pearlitic grades, but their ductility is slightly lower than the ferritic grades. These materials also satisfy the requirements for the strength of the quenched and tempered grades and their ductility is superior to this grade. The correlation between the strain-hardening rates of the various austempered ductile iron (ADI) with DMS and conventionally heat-treated ADI microstructures as a function of strain was conducted by inspection of the respective tensile curves. For this purpose, the Crussard-Jaoul (C-J) analysis was employed. The test results also indicate that strain-hardening behavior of ADI with dual matrix is influenced by the variations in the volume fractions of the phases, and their morphologies, the degree of ausferrite connectivity and the interaction intensities between the carbon atoms and the dislocations in the matrix. The ADI with DMS generally exhibited low strain-hardening rates compared to the conventionally ADI.

Keywords ausferrite volume fraction, austempered ductile iron (ADI), dual matrix structure (DMS), new ferrite volume fraction, partial austenitizing, proeutectoid ferrite volume fraction, strain-hardening

1. Introduction

With increasing applications as a substitute for forged steels in manufacturing industries, austempered ductile iron (ADI) has vital importance in the evaluation of the strain-hardening behavior of ADI. In many applications, ADI components undergo substantial plastic strains (e.g., fatigue, wear). The mechanical behaviors of these components are, therefore, influenced by the strain-hardening characteristics of the material.

To correlate the strain-hardening behavior with microstructures, the flow curve during the uniform plastic deformation is commonly analyzed with the aid of some idealized mathematical stress-strain equations. The most common of them is the Holloman equation, $\sigma = K\varepsilon^n$, or Log σ = log $K + n$ log ε which is widely used to describe the strain-hardening behavior of metals and alloys under the plastic deformation. (Here σ stands for the true stress, ε the true strain, K the strength coefficient, and n is the strain-hardening exponent (or n value) of the material.)

The strain-hardening behavior can be evaluated by determining the n value of the ductile iron. The strain-hardening exponent of an alloy is an important parameter because it defines the strain-hardening capacity of the material when it is plastically deformed. A high n value indicates a more uniform strain distribution which results in a greater resistance to necking. When the materials display a single value of n up to necking, which corresponds to the UTS, n should be equal to the true strain at necking. A log-log plot of true stress and true strain up to maximum load will result in a straight line with n as slope. Accordingly, double logarithmic plots are frequently used as a measure of the suitability of particular mathematical stress-strain equation to describe the strain-hardening behavior.

Using the Holloman equation, Yang et al. (Ref 1) analyzed the strain-hardening behavior of ADI subjected to a novel two-step austempering process. They showed that the strain-hardening exponent values of ADI with two-step austempering process resulted in a lower ductility and the strain-hardening exponent values, compared to the conventional single-step austempering process. This result was attributed to a function of amount and morphology of microstructural constituents and the interaction intensities between carbon atoms and dislocations in the matrix.

Volkan Kilicli and **Mehmet Erdogan,** Materials Division, Metallurgy Education Department, Faculty of Technical Education, Gazi University, Besevler-Ankara 06500, Turkey. Contact e-mail: mehmeter@gazi.edu.tr.

In the complex structures, the relationship between the tensile stress (σ) and the strain (ε) is, in general, no longer well described by a single exponent Holloman-type equation, particularly, when one of the phases such as austenite is unstable during the deformation (Ref 2).

Using the Holloman equation, Aranzabal et al. (Ref 2) analyzed deformation behavior of conventional ADI. In their work, ln σ vs. ln (ε) was adopted, and a single or double n method ε_p^n was used to describe the experimental data. They found a TRIP effect increasing the strain-hardening, which produces a change in the slope of the Holloman equation.

Apart from the Holloman relationship, the other mathematical expressions have also been used for detecting transition in deformation behavior, because they reflect discontinuities in the curvature of the stress-strain curve. One such expression is the Crussard-Jaoul analyses based on Ludwik equation: $\sigma = \sigma_o + K\varepsilon_p^n$ or $\log(d\sigma/d\varepsilon) = \log K + \log n + (n-1)\log \varepsilon$. (Here σ stands for the true stress, ε_p the true strain, σ_o, K, and n are constants).

In these analyses, n and K values are determined from the slope of a log $d\sigma/d\varepsilon_p$ against log ε curve.

Very limited works related to the strain-hardening characteristics of conventional ADI are available in the literature (Ref 1, 2) and, moreover, the strain-hardening behavior of ADI with dual matrix structure (DMS) (it is also called the newly developed iron) (Ref 3-16) has not been reported yet. In the newly developed ductile cast iron with DMS, the structure consists of proeutectoid ferrite, and martensite or ausferrite (bainitic ferrite and austenite). Therefore, it is also called the DMS.

Recently, it has been shown that the proof and tensile stresses of the newly developed iron are significantly higher than the pearlitic and ferritic grades. The ductility is lower than the ferritic grades, but it remains adequate for the most applications (Ref 11-13). ADI with DMS is an attractive material for some applications such as automotive suspension parts where a good combination of high strength and ductility is required (Ref 5).

The aim of the current investigation is to examine how the variation in the microstructural parameters affects the strain-hardening behavior of ADI with DMS and conventionally heat-treated ADI.

2. The Experimental Procedure

The chemical composition and microstructure of as cast unalloyed ductile iron used in the present study is given in Table 1. Two different starting microstructures were obtained by as cast and oil quenching following austenitization at 900 °C for 20 min. As-cast material had ferrite + graphite structure (Fig. 1). This microstructure was labeled as "A" for further reference. Oil quenching produced a microstructure that was almost wholly martensitic (Fig. 2). This was labeled as "B". The microstructures of specimens A and B were the starting point for the subsequent austempering heat treatment. As-cast samples were also heat-treated at the conventional austenitizing temperature of 900 °C in single-phase region (γ) and then austempering was carried out at the austempering temperature of 365 °C for comparison. Figure 3 provides a summary of the heat treatments.

Those starting microstructure of series A and B were intercritically austenitized (partially austenitized) in two-phase regions ($\alpha + \gamma$) at various temperatures of 795, 815, and 830 °C for 20 min and then quenched into salt bath held at austempering temperature of 365 °C for various times to obtain various ausferrite volume fractions and their morphologies. The details of casting, heat treatment procedure, x-ray analysis, specimen preparations, and testing methods are given elsewhere (Ref 15, 16).

The specimens were coded according to the starting microstructure and intercritical austenitizing temperature (ICAT). For example, in specimen code A815, A stands for the starting microstructure and 815 for the ICAT. On the other hand, the conventionally heat-treated sample is coded as C900. The results of phase proportions are listed in Table 2.

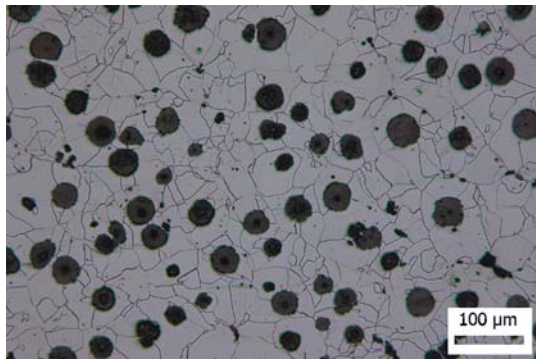

Fig. 1 Starting microstructure of as-cast ductile iron. Etchant: 2% Nital

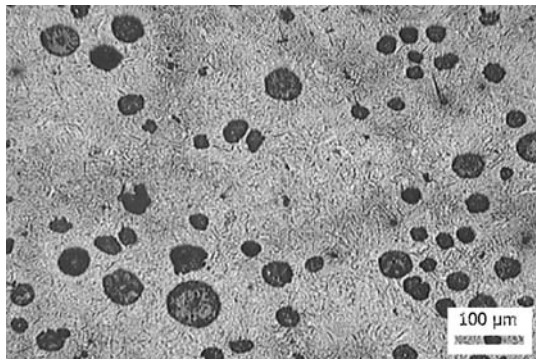

Fig. 2 Starting microstructure of quenched sample from 900 °C. Etchant: 2% Nital

Table 1 Chemical composition of unalloyed ductile iron used (wt.%)

C	Si	Mn	P	S	Mg	Cu	Ni	Cr	Mo	Al	Fe
3.5	2.63	0.318	0.019	0.009	0.0471	0.0552	0.0423	0.031	0.0421	0.003	Rest

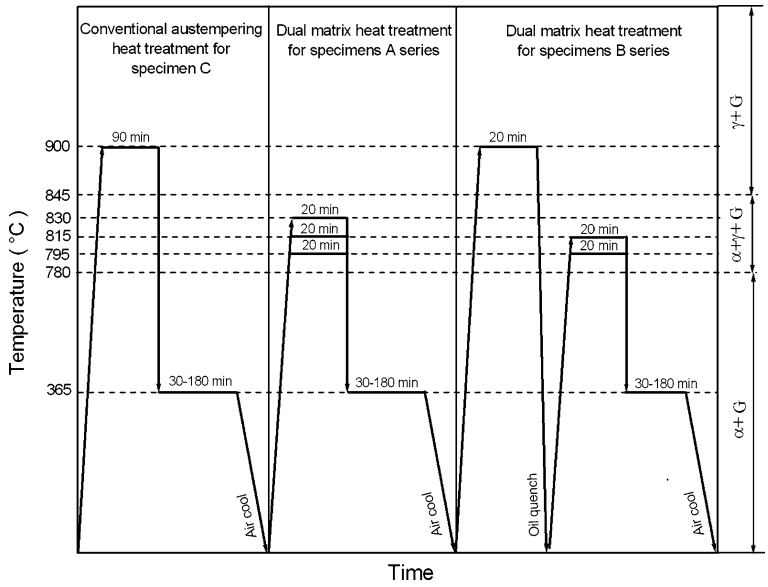

Fig. 3 Summary of heat treatments

3. Results and Discussions

3.1 The Heat Treatments and Microstructures

The austempering at the 365 °C for 120 min from the conventional heat treatment temperature of 900 °C produced a typical ausferritic structure throughout the specimen C900 (Fig. 4).

The austempering from different ICAT of 815 or 795 °C produced a DMS consisting of ausferrite and proeutectoid ferrite at the specimens with different ausferrite volume fractions (AFVF) restricted to eutectic cell boundaries and to an isolated or continuous network of ausferritic structure along the eutectic cell boundary formed depending on AFVF (Fig. 5a-e). The eutectic cell boundaries are the potent sites for the austenite nucleation. In series B, specimen with martensitic starting microstructure, ausferrite structure is more uniformly and finely distributed along the eutectic cell boundaries (Fig. 5d, e) when compared with series A specimens (Fig. 5a, b) under the same austempering conditions. The martensitic starting microstructure has a number of precipitation sites such as the plate interfaces, plate colony boundaries and prior austenite grain boundaries for the austenite to form, and thus, a more finely dispersed austenite is obtained (Ref 11, 17).

The notable feature of the intercritical austenitizing heat treatment compared with the conventional austenitizing heat treated ones is that in the austenite + ferrite region, the austenite volume fraction and its carbon content depend on the ICAT. When the ICAT increases, the austenite volume fraction and its carbon content increase, and proeutectoid ferrite volume fraction (PFVF) decreases as defined by the lever rule (Ref 15, 16).

Before the austempering from ICAT, this feature provides the adjustment of the parent austenite volume fraction and its carbon content, and proeutectoid ferrite volume fraction at the ICAT. The parent austenite carbon content has an effect on high-carbon austenite stabilization during the austempering. Therefore, in the intercritically austenitized materials, the potential exists to influence the austenite stabilization during the austempering. At the constant 120 min austempered time, the variation of carbon content in the austenite with the austenitizing temperature obtained by X-RD analyses is given in Fig. 6. The austenite carbon content increased with the increasing austenitizing temperature. This result is in good agreement with the existing literature (Ref 18, 19).

Some examples of the result of quantitative metallographic analysis of series A, B, and C are shown in Fig. 7a-c in the form of quantitative microstructure maps. The austempering times and phase proportions in all specimens are given in Table 2. In all the series, increasing the austempering time caused the displacement of martensite with the bainitic ferrite and high-carbon austenite.

The details of the results and discussions of the heat treatments and microstructures and quantitative metallographic analysis are given elsewhere (Ref 15, 16).

3.2 The Tensile Properties

Since the maximum properties in the austempered samples were achieved at times corresponding to the processing window (Fig. 7a-c and Table 2), the discussion was focused on the structure-tensile property relationships in the samples austempered for 120 min.

The stress-strain curves of samples austempered for 120 min are shown in Fig. 8. The variation in the 0-2% proof and the tensile strength and uniform and total elongation with AFVF are given in Fig. 9 and 10. The conclusions of the tensile properties are briefly outlined as follows:

- The ADI with the DMS exhibits much greater ductility than the conventionally ADI.
- The proeutectoid ferrite and the ausferrite volume fractions can be controlled to influence the strength and the ductility of the ADI with the DMS.
- For a wide combination of intercritical austenitizing and austempering times, the tensile strength and ductility can be satisfactorily optimized.

Table 2 Results of metallographic measurement and tensile properties (Average values ±3)

Specimens code	Austemp. time, min	High carbon austenite content, vol.%		Bainitic ferrite content, vol.%		Proeutectoid ferrite content, vol.%		Martensite content, vol.%		New ferrite content, vol.%		0.2 % Proof stress, MPa		Tensile strength, MPa		Uniform elongation, %		Total elongation, %		Hardness, HV 5	
		Seri A	Seri B	Seri A	Seri B	Seri A	Seri B	Seri A	Seri B	Seri A	Seri B	Seri A	Seri B	Seri A	Seri B	Seri A	Seri B	Seri A	Seri B	Seri A	Seri B
795A and 795B	30	3.1	9.3	5.9	16.7	75.3	49.5	14.2	24.5	1.5	...	272.9	369.4	406.3	522.4	20.1	12.6	25	12.6	210	220
	60	5.8	15.8	7.6	19.9	75.3	49.5	6.6	14.8	4.7	...	320.2	359.4	456.5	493	21.3	13.6	26	13.6	195	202
	120	8.1	24.8	8.9	25.7	75.3	49.5	0	0	7.7	...	306.3	373.2	440.6	534.3	22.9	13.7	27.5	13.7	180	204
	180	7.1	24.1	7.9	26.4	75.3	49.5	0	0	9.7	...	325.3	384.4	460.5	541.4	19.4	12.4	24.5	12.4	205	208
815A and 815B	30	7.9	15.2	8.3	20.3	38.2	35	38.2	25.5	7.4	...	345.8	570.2	481.2	721.9	14.3	9.7	18	9.7	265	287
	60	13.8	21.8	14.6	27.3	38.2	35	23.2	14.9	10.2	...	385.1	558.3	552	709.5	15	10.8	19.7	10.8	253	273
	120	22.5	31.2	24.7	33.8	38.2	35	0	0	14.6	...	370.2	588.3	529	732.5	18.6	12.8	22.7	12.8	228	248
	180	22.3	29.5	24.4	35.5	38.2	35	0	0	15.1	...	379.6	599.1	532.6	740.1	17.4	11.6	20	11.6	240	260
830A[a]	120	27.1		32.9		21.8		0		18.2		518		685.4		13.6		15		267	
900C	30	19.3		28.1		...		52.6		...		816		1111.1		3		3		345	
	60	28.5		37.9		...		33.6		...		784		1089.9		10.6		10.6		324	
	120	39.3		55.2		...		5.5		...		778		1085.7		12.1		12.1		302	
	180	37.8		62.2		...		0		...		810		1105.1		10		10		315	
As-cast	...	...		...		89.8		...		...		261.5		297		22.7		27.7		175	

[a]A full test program would have required 30, 60, 120, and 180 min austempering for A 830 and B 830 specimens. In practice, material constraints limited the 30, 60, 180 min austempering for A 830 specimen and 30, 60, 120, and 180 min austempering for B830 specimen were missing from the dataset

Fig. 4 Microstructure of conventionally heat-treated specimen C900 showing a typical ausferritic structure after austempering for 120 min. Etchant: 2% Nital

- The new ferrite is an identifiable, controllable parameter and influences the tensile behavior in an unalloyed ductile cast iron.
- The new ferrite formation depends on the prior (parent) austenite dispersion at ICAT and the austempering time. Only the coarse parent austenite dispersion produces the new ferrite during the austempering.
- The new ferrite volume fraction increases with the increasing ICAT and the austempering time.
- The finer parent austenite dispersion produces more high-carbon austenite than the coarse one for the same austempering time.
- The specimen with ~47.2% ausferrite volume fraction (coarse structure) exhibited the best combination of high strength and ductility. The strength and ductility of this material is much higher than the ferritic grades and its strength is at the same level as the pearlitic grades, but the ductility is almost four times as high as the pearlitic grades.
- Compared to the pearlitic grades, both of the specimens with ~75% ausferrite volume fraction (coarse structure) and the specimen with ~82% ausferrite volume fraction (fine structure) exhibited the best combination of high strength and ductility, but their ductility is slightly lower than the ferritic grades. These materials also satisfy the requirements for the strength of the quenched and the tempered grades and their ductility is superior to this grade.

3.3 The Strain-Hardening Behavior

The correlation between the strain-hardening rates of the ADI with various dual matrix microstructures and conventionally heat-treated ADI as a function of strain was conducted by inspection of the respective tensile curves. For this purpose, the Crussard-Jaoul (C-J) analysis was employed. C-J plots are presented in Fig. 11a-c.

Figure 11 shows that while as cast specimen and series A specimens with DMSs exhibited three stages of hardening (Fig. 11a) and series B specimens with DMSs (Fig. 11b) and conventionally austempered specimen (Fig. 11c) exhibited two stages of hardening with the stages covering (1) ~0.03-0.06; (2) ~0.06-0.15; and (3) ~0.15-0.24% total strain. With respect to these hardening stages, intercept and slope values were

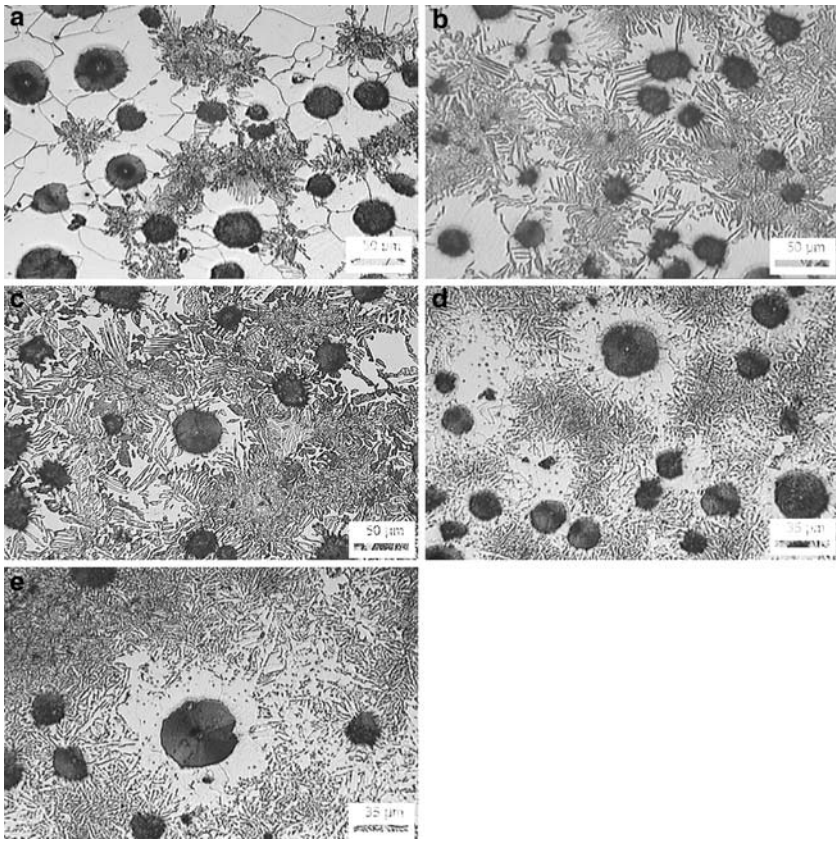

Fig. 5 The microstructures of specimen (a) A795 (17AFVF), (b) A815 (47.2AFVF), (c) A830 (75 AFVF), (d) B795 (50.5 AFVF) and (e) B 815(65 AFVF) austempered for 120 min. Etchant: 2% Nital. $\alpha_b + \gamma_{hc}$: Ausferrite (bainitic ferrite + high carbon austenite), α_p: Proeutectoid ferrite

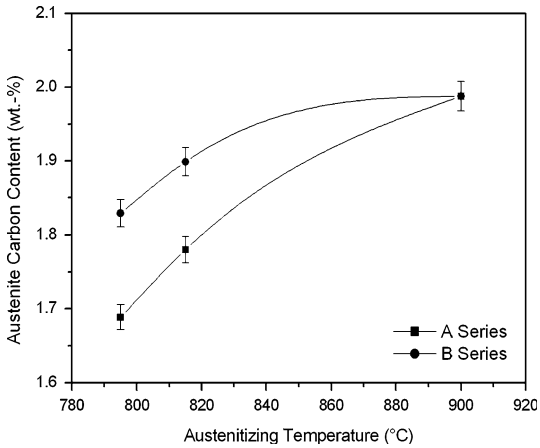

Fig. 6 At the constant 120 min austempering time, X-RD analyses of specimens showing the variation of austenite carbon content with austenitizing temperature

determined by linear regression analysis. The results of this analysis are given in Table 3.

As can be seen from Fig. 11a, the strain-hardening rate in series A specimens decreased in three stages. The most rapid decrease in strain-hardening rate occurred in Stage 1, and Stage 1 continued to higher strains.

The most notable feature of Fig. 11a, b is that Stage 2 started at a lower strain-hardening rate and at a higher strain, and decreased more slowly with increasing strain for each dual matrix microstructural condition, and this decrement was higher in series A specimens (Fig. 11a and Table 3) compared to series B specimens (Fig. 11b and Table 3).

The strain-hardening rate of series A specimens in Stage 3 decreased very slowly with strain and converged to low values.

The strain-hardening phenomenon in DMS of ferrous alloys generally has been found to be a function of the microstructure and the volume fraction of the second phase (Ref 1, 2, 20, 21). It was generally agreed that the mean free path of dislocation motion controls strain-hardening behavior.

In the first stage, the rate at which the strain-hardening rate decreased with respect to strain was mainly dependent on the microstructural variations in ADI with DMSs (i.e., the effect of proeutectoid, new and bainitic ferrites and high-carbon austenite contents and their morphologies and degree of ausferrite connectivity on the homogeneity of deformation behavior) and, therefore, the stress-strain curves were different at low strains.

When the strain-hardening rate of series A and B specimens austempered from the same ICAT were compared with each other (i.e., A795 and B795), series B specimens had higher strain-hardening rate in Stage 1 than series A specimens. These results may be attributable to the absence of high deformable new ferrite and less proeutectoid and bainitic ferrite and high-ausferrite volume contents and fine structure in series B specimens. In ADI with DMS having fine ausferrite morphology, strain-hardening rate was found to be dependent on starting microstructure. Fine starting microstructure results in fine ausferrite structure and fine parent austenite dispersion

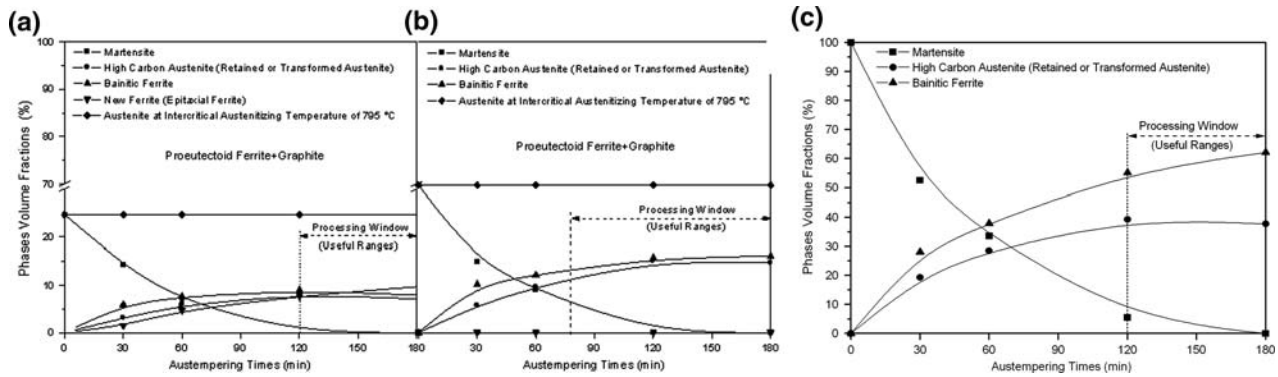

Fig. 7 Quantitative microstructure maps showing effect of austempering times on the microstructure of series (a) A and (b) B austempered for various times from partially austenitizing temperature of 795 °C and conventionally austempered from austenitizing temperature of (c) 900 °C

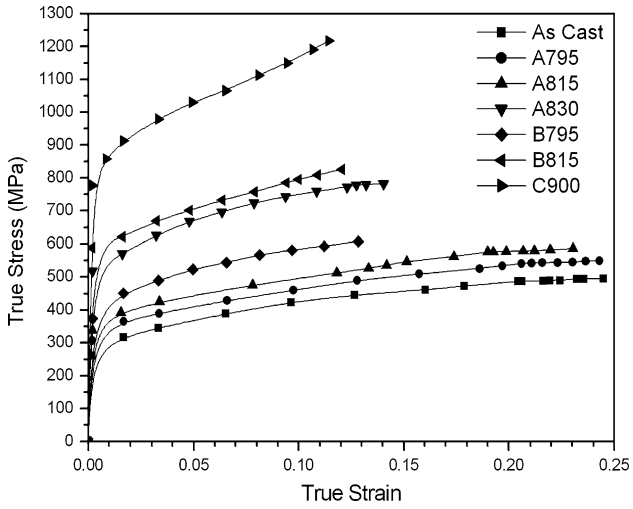

Fig. 8 True stress-strain curves for specimens austempered for 120 min

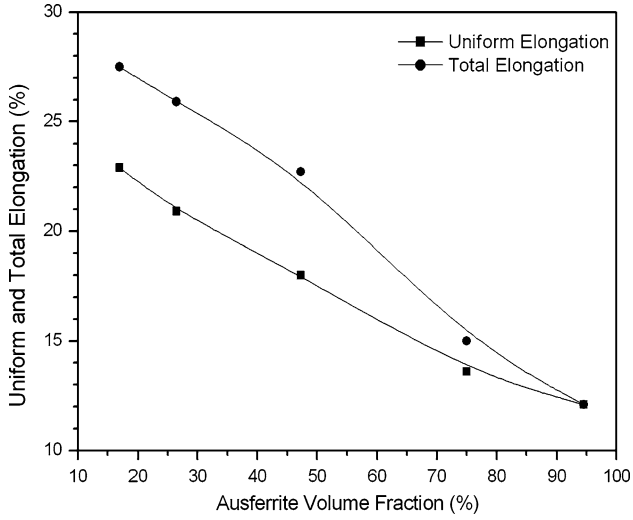

Fig. 10 The relationship between ausferrite volume fraction and uniform and total elongations of various series A specimens after austempering for 120 min

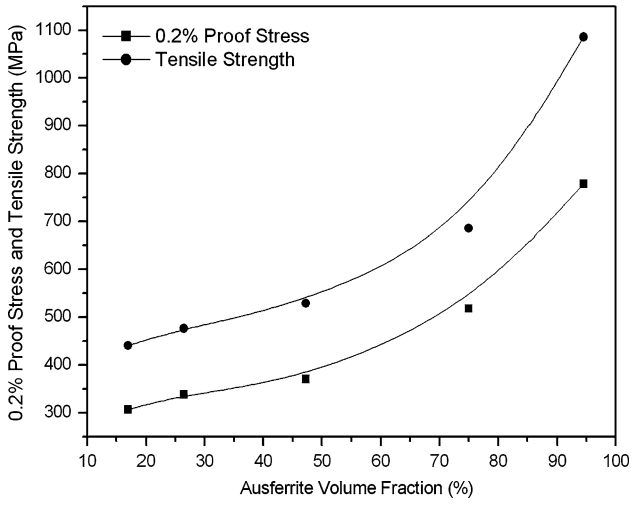

Fig. 9 The relationship between ausferrite volume fraction and 0.2% proof and tensile strengths of series A specimens after austempering for 120 min

produces higher-carbon austenite than coarse ones following austempering for a given time from ICAT range (Ref 15, 16).

The increment in the volume fraction of new ferrite could cause more inhomogeneous deformation due to its higher deformability than proeutectoid ferrite (Ref 22-28). The effect of new ferrite, in series A with dual matrix microstructures, on reducing the strain-hardening rate might result from its effect in increasing ductility. New ferrite has been reported to be free of precipitations (Ref 23). Recently, it has been shown that new ferrite in ADI with DMS is an identifiable, controllable parameter and influences tensile behavior and new ferrite formation depends on prior (parent) austenite dispersion at ICAT and austempering time. Only coarse parent austenite dispersion produces new ferrite during austempering and new ferrite volume fraction increases with increasing ICAT and austempering time (Ref 15, 16).

As defined by lever rule, parent austenite volume fraction and its carbon content decreases with decreasing ICAT. As a consequence, AFVF and connectivity between ausferrite particles in ferrite matrix decreases with decreasing ICAT after austempering for a given austempering time from ICAT range.

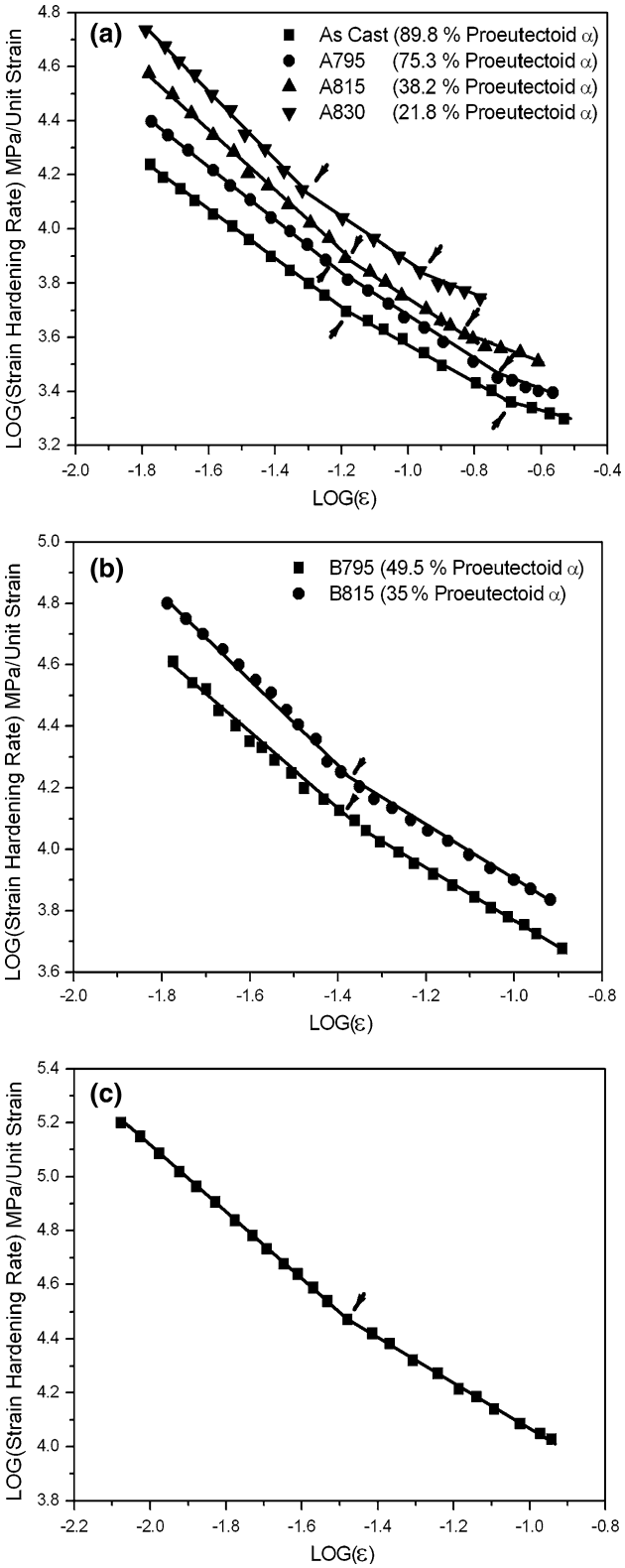

Fig. 11 The plot for the analysis of the strain-hardening behavior of (a) series A, (b) series B and (c) conventionally austempered specimen

In the specimens austempered from lowest ICAT of 795 °C, the volume fraction of ferrite (proeutectoid + new and bainitic ferrite) in series A specimens and proeutectoid and bainitic ferrite in series B specimens was considerably larger than high-carbon austenite volume fraction. Therefore, ductile ferrite may play a dominant role to control the strain-hardening behavior as a matrix structure.

As mentioned before, in this study, austempering from different ICAT produced ausferritic structure with different AFVF restricted to eutectic cell boundaries and an isolated or continuous network of ausferritic structure along the intercellular boundary depending on AFVFs. In specimens with the higher degree of ausferrite connectivity, ferrite around graphite nodules were completely surrounded by ausferritic structure as shown in Fig. 5b-e. In those microstructures, high-strength ausferritic structure may restrict deformation of low-strength ferrite under tensile loading and ductility decreases with increasing continuity of ausferritic structure along eutectic cell boundaries (Ref 15, 16). In this case, uniform plastic flow is expected to occur in a smaller fraction of the total volume of the ferrite matrix, causing more inhomogeneous deformation. Likewise, in the present work, the strain-hardening rate in Stage 1 decreased with a decreasing degree of ausferrite connectivity and increasing proeutectoid, new and bainitic ferrite contents.

The strain-hardening is believed to be as a consequence of dislocation multiplication and interaction. It has been shown that the ferrite laths in ADI contain dislocations (Ref 29). In addition to dislocations, interactions solute atoms should also contribute to the strain-hardening effect. For this reason, both the interactions between dislocations and carbon atoms in ferrite may have contributed to the strain-hardening effect in ADI with DMS.

Austempering from higher ICAT resulted in high volume fraction of ausferrite for a given austempering time and more bainitic ferrite grain boundaries existed in ausferritic structure behaving as a dislocation source, so the total dislocation densities were higher. In such structure, the interactions between dislocations and carbon atoms are expected to be high compared to those specimens austempered from low ICAT and this has contributed to the relatively higher values of strain-hardening exponent in ADI with DMS.

On the other hand, in the present study, coarser bainitic ferrite and austenite particles were formed in series A specimens (Fig. 5b) compared to series B specimens (Fig. 5e) leading to decrease in the interface areas and an increase in the mean free path of dislocation in the large bainitic ferrite particle size in series A specimens. During deformation, the interfaces between particles serve as an obstacle for dislocation motion and dislocation sources. With the decrease in the interface areas in series A specimens, reduced numbers in dislocation sources and obstacles to dislocation motion compared to series B specimen with fine ausferrite structure have led to weaker interactions between carbon atoms and dislocations. As a result, strain-hardening rate decreased.

In the series A and B specimens, the strain-hardening mechanism is the same. The differences between both series here is that series B specimen generated higher carbon austenite under the same austempering conditions (Ref 16); therefore, the volume fraction of proeutectoid ferrite was lower in series B specimens. The reduction in proeutectoid ferrite content, absence of new ferrite and finer ausferritic structure resulted in higher strain-hardening rates and two stages of strain hardening for series B specimens.

However, results indicate that among the three dominant microstructural features of ferrite (particle size, volume

Table 3 The slope, intercept and strain values according to deformation stages of the specimens in the Swift equation estimated by the modified C–J analysis

			$y = mx + n$								
			Stage I			Stage II			Stage III		
Specimen code	New ferrite, %	Proeutectoid ferrite, %	Slope (m)	Intercept (n)	ε, %	Slope (m)	Intercept (n)	ε, %	Slope (m)	Intercept (n)	ε, %
As cast	...	89.8	–0.850	2.766	0.066	–0.808	2.816	0.160	–0.830	2.798	0.244
A795	7.7	75.3	–0.902	2.747	0.065	–0.802	2.865	0.157	–0.826	2.846	0.242
A815	14.6	38.2	–0.866	2.863	0.064	–0.792	2.951	0.134	–0.829	2.918	0.204
A830	18.2	21.8	–0.855	3.015	0.047	–0.835	3.041	0.078	–0.865	3.008	0.140
B795	...	49.5	–0.861	2.899	0.049	–0.843	2.923	0.128	...	...	...
B815	...	35	–0.886	2.995	0.048	–0.822	3.080	0.120	...	...	...
C900	...	...	–0.903	3.133	0.033	–0.824	3.250	0.114	...	...	...

fraction, and dislocation density), probably the volume fraction of ferrite is the most predominant factor to control strain-hardening behavior of ADI.

Further increase in ICAT in series A, specimen caused substantial reduction in the ferrite volume fraction (Table 2). Therefore, the dominant effect of ferrite volume fraction on the strain-hardening rate greatly decreased.

In the case of specimen A830 and B815 austempered from ICAT of 830 and 815 °C, respectively, the volume fraction of ausferrite in both specimens became large enough to replace proeutectoid ferrite matrix to play the dominant role in controlling strain-hardening behavior of ADI with DMS. Austenite has a higher strain-hardening capacity than ferrite (Ref 1). Therefore, the higher strain-hardening capacity of austenite compensated partly the decrease of strain-hardening effect of ferrite (Fig. 11). When the ausferrite becomes matrix, it is reasonable to expect that the contribution to strain-hardening from the interactions between dislocations and carbon atoms will be minimum. With increasing volume fraction of ausferrite, the transition between the respective deformation stages shifted to earlier strains.

The specimen C 900 exhibited two stages of strain-hardening Fig. 11c. Austempering for 120 min from conventional austenitizing temperature of 900 °C corresponding to single-phase region of austenite produced almost ausferritic structure throughout the specimen (Fig. 4). In this case, larger volume fraction of high-carbon austenite will result in higher strain-hardening effect for ADI. Since the carbon content of parent austenite present at conventional austenitizing temperature is higher than that of austenite present at ICAT range as defined by the lever rule, austenite becomes coarser in nature, the interactions between carbon atoms and dislocations will also have contributions to the strain-hardening rate of ADI.

In conventionally austempered samples, in addition to the contribution of high volume fraction of austenite and its high carbon content to the strain-hardening rate, strain-induced martensite transformation during deformation may be contributed to the strain-hardening rate. Before straining, conventionally austempered specimen already contains 5.5% martensite (Table 2). In addition to this martensite, total martensite content may further increase by strain-induced martensite during deformation since high-carbon content austenite may still transform into martensite depending on efficiency of applied strain (Ref 30) and causes the hardening of the material (Ref 31-33); thus, strain-hardening rate increases.

The ADI with DMS austempered from ICAT range did not contain martensite after austempering for 120 min (Fig. 7 or Table 2). The advantage of further strain-hardening effect of higher austenite content was not realized because of their low-ausferrite content; thus, limited the formation of strain-induced martensite. In this case, strain-hardening mechanism in austenite by martensite transformation did not function completely. As can be seen from Table 2 that the maximum ductility produced by DMS heat treatment process was considerably higher than the conventionally heat-treated ADI. Therefore, the strain-induced martensite would be very limited in ADI samples processed by the current DMS heat treatment process.

It can be concluded that to control strain-hardening behavior of material, this novel heat treatment process for ADI to produce DMS has more microstructural variables than conventional austempering process. The strain-hardening behavior of ADI with DMS can be controlled by varying content of microstructural constituents such as ferrite (proeutectoid ferrite, new ferrite, bainitic ferrite, and high-carbon austenite) and their morphologies. Conventionally heat-treated ADI has no such advantages.

Other investigators (Ref 24, 34, 35) have used the C-J analysis to characterize the stress-strain curves of a number of dual-phase steels. Cribb and Rigsbee (Ref 34) proposed the existence of three stages of work-hardening behavior. They determined the limits of stages to be 0.1-0.5, 0.5-4 and 4-18% strain. With increasing volume fraction of martensite, the transition between the respective deformation stages shifted to earlier strains. Matlock et al. (Ref 35) correlated the transition from a steep, continuous to shallow, discontinuous C-J slope with a decrease in cooling rate, annealing temperature and volume fraction of martensite, or an increase in aging time and grain size. They attributed the presence of distinct inflexion points to an increase in the degree of inhomogenity in the deformation of the sample associated with inhomogenity of dislocation structure produced by varying processing parameters. Lawson et al. (Ref 24) observed similar families of curves as the cooling rate decreased.

4. Conclusions

A novel heat-treatment process for ADI to produce DMS was carried out. This heat-treatment process produced remarkable variations in the proeutectoid, new and bainitic ferrites and high-carbon austenite contents and strain-hardening behavior at two levels of microstructural refinement. The most important of these are briefly outlined as follows:

1. The strain-hardening rate in series A specimen having new ferrite and coarse structure decreased with strain in three stages. On the other hand, the strain-hardening rate in series B specimen with no new ferrite and fine structure decreased with strain in two stages. In both series A and series B structure the strain-hardening rate decreased most rapidly in the first of these stages, slowly in Stage 2, and more slowly again in Stage 3.
2. Strain-hardening behavior of ADI with DMS is influenced by the variations in the volume fractions of phases, and their morphologies, the degree of ausferrite connectivity and interaction intensities between carbon atoms and dislocations in the matrix.
3. Strain-hardening rate increases with increasing ausferrite volume fraction or decreasing proeutectoid and new ferrite volume fractions.
4 .As the proeutectoid ferrite content was increased, Stage 2 started at a lower strain-hardening rate and at a higher strain, and decreased more slowly with increasing strain for each dual matrix microstructural condition.
5. In ADI having DMS, the strain-hardening rate decreased with a decrease in degree of ausferrite connectivity in the proeutectoid ferrite matrix.
6. The interactions between dislocations and carbon atoms are influenced by the interface areas. With increase in the interface areas in the case of series B specimens with fine ausferritic structure, the interactions between dislocations and carbon atoms became stronger; consequently, the strain-hardening rate increased compared to series A specimens with coarse structures.
7. The effect of new ferrite, in series A with dual matrix microstructures, on reducing the strain-hardening rate was responsible for its effect in increasing ductility.
8. To control strain-hardening behavior of material, novel heat treatment process for ADI to produce DMS has more microstructural variables than conventional austempering process. The strain-hardening behavior of ADI with DMS can be controlled by varying content of microstructural constituents (proeutectoid + new and ferrite and high-carbon austenite) and their morphologies and degree of ausferrite connectivity in the proeutectoid ferrite matrix.

Acknowledgments

The authors wish to acknowledge the financial supports of Gazi University Scientific Research Fund (Project Code 07/2003-41 and 07/2005-25). The author is also indebted to ALFA Casting Company (Ankara, Turkey) for castings and to Ankara Nuclear Research and Education Center (TAEK-ANAEM) for providing X-Ray facilities. My acknowledgements are also extended to the UMIST Manchester Materials Science Centre for the provision of its laboratory facilities and to its staff who have assisted me throughout our study.

References

1. J. Yang and S.K. Putatunda, Influence of a Novel Two-Step Austempering Process on the Strain-Hardening Behavior of Austempered Ductile Cast Iron (ADI), *Mat. Sci. Eng. A*, 2004, **A382**(1–2), p 265–279 in English
2. J. Aranzabal, I. Gutierrez, J.M. RodriguezIbabe, and J.J. Urcola, Influence of the Amount and Morphology of Retained Austenite on the Mechanical Properties of an Austempered Ductile Iron, *Met. Mat. Trans. A*, 1997, **28A**(5), p 1143–1156 in English
3. R.C. Voigt, L.M. Eldoky, and H.S. Chiou, Fracture of Ductile Cast Irons With Dual Matrix Structure, *AFS Trans.*, 1986, **94**, p 645–656 in English
4. A.M. Rashidi and M. Moshrefi-Torbati, Effect of Tempering Conditions on the Mechanical Properties of Ductile Cast Iron with Dual Matrix Structure (DMS), *Mat. Let.*, 2000, **45**(3–4), p 203–207 in English
5. J. Aranzabal, G. Serramoglia, and D. Rousiere, Development of a New Mixed (Ferritic-Ausferritic) Ductile Iron for Automotive Suspension Parts, *Int. J. Cast. Met. Res.*, 2003, **16**(1–3), p 185–190 in English
6. T. Kobayashi and H. Yamamoto, Development of High Toughness in Austempered Type Ductile Cast Iron and Evaluation of its Properties, *Metall. Mat. Trans. A*, 1988, **19A**(2), p 319–327 in English
7. T. Kobayashi and S. Yamada, Effect of Holding Time in the ($\alpha + \gamma$) Temperature Range on Toughness of Specially Austempered Ductile Iron, *Metall. Mat. Trans. A*, 1996, **27A**(7), p 1961–1971 in English
8. Z.R. He, G.X. Lin, and S. Ji, Deformation and Fracture Behaviour of Cast Iron with Optimized Microstructure, *Mat. Charac.*, 1997, **38**(4–5), p 251–258 in English
9. M. Hafiz, Tensile Properties and Fracture of Ferritic SG-Iron having Different-Shell Structure, *Z. Metallkd.*, 2001, **92**(11), p 1258–1261 in English
10. R. Kazerooni, A. Nazarboland, and R. Elliot, Use of Austenitising Temperature in Control of Austempering of An Mn-Mo-Cu Alloyed Ductile Iron, *Mat. Sci. Tech.*, 1997, **13**(12), p 1007–1015 in English
11. M. Cerah, K. Kocatepe, and M. Erdogan, Influence of Martensite Volume Fraction and Tempering Time on Tensile Properties of Partially Austenitized in the ($\alpha + \gamma$) Temperature Range and Quenched + Tempered Ferritic Ductile Iron, *J. Mat. Sci.*, 2005, **40**(13), p 3453–3459 in English
12. M. Erdogan, K. Kocatepe, and M. Cerah, Influence of Intercritical Austenitising and Tempering Time and Martensite Volume Fractions on Tensile Properties of Ferritic Ductile Iron with Dual Matrix Structure, *Int. J. Cast. Met. Res.*, 2006, **19**(4), p 248–253 in English
13. K. Kocatepe, M. Cerah, and M. Erdogan, The Tensile Fracture Behaviour of Intercritically Annealed and Quenched + Tempered Ferritic Ductile Iron with Dual Matrix Structure, *Mat. Design*, 2006, **28**(1), p 172–181 in English
14. M. Erdogan, V. Kilicli, and B. Demir, Transformation Characteristics of Ductile Iron Austempered from Intercritical Austenitizing Temperature Ranges, *J. Mat. Sci.*, in Press, DOI: 10.1007/s10853-006-1415-7, 2007, in English
15. V. Kilicli and M. Erdogan, Tensile Properties of Partially Austenitized and Austempered Ductile Irons with Dual Matrix Structures, *Mat. Sci. Tech.*, 2006, **22**(8), p 919–928 in English
16. V. Kilicli, and M. Erdogan, The Effect of Ausferrite Volume Fraction and its Morphology on the Tensile Properties of Partially Austenitized and Austempered Ductile Irons with Dual Matrix Structures, *Int. J. Cast. Met. Res.* 2006, Submitted, in English
17. C.R.F. Azevedo, A.A. Garboggini, and A.P. Tschipitschin, Effect of Austenite Grain Refinement on Morphology of Product of Bainitic Reaction in Austempered Ductile Iron, *Mater. Sci. Tech.*, 1993, **9**(8), p 705–710 in English
18. C.S. Roberts, Effect of Carbon on the Lattice Parameter of Austenite, *Trans. AIME*, 1953, **197**, p 203–204 in English
19. K.B. Rundman and R.C. Klug, X-ray and Metallographic Study of an Austempered Ductile Cast Iron, *AFS Trans.*, 1982, **90**, p 499–508 in English
20. A.M. Sarosiek and W.S. Owen, Work Hardening of Dual-Phase Steels at Small Plastic Strains, *Mater. Sci. Eng. A*, 1984, **66**(1), p 13–34 in English
21. Z. Fan, H. Mingzhi, and S. Deke, The Relationship Between the Strain-Hardening Exponent n and the Microstructure of Metals, *Mater. Sci. Eng. A*, 1989, **122**(2), p 211–213 in English
22. G.S. Huppi, D.K. Matlock, and G. Krauss, An Evaluation of the Importance of Epitaxial Ferrite in Dual Phase Steel Structure, *Scrip. Met.*, 1980, **14**(11), p 1239–1243 in English
23. M.D. Geib, D.K. Matlock, and G. Krauss, The Effect of Intercritical Annealing Temperature on the Structure of Niobium Microalloyed Dual Phase Steel, *Metall. Trans. A*, 1980, **11A**(10), p 1683–1689 in English

24. R.D. Lawson, D.K. Matlock, and G. Krauss, The Effect of Microstructure on the Deformation Behavior and Mechanical Properties of a Dual-Phase Steel, *Fundamentals of Dual-Phase Steels*, R.A. Kot and B.L. Bramfitt, Ed., AIME, Warrendale, 1981, p 347–381
25. M. Erdogan, The Effect of New Ferrite Content on the Tensile Fracture Behaviour of Dual Phase Steels, *J. Mat. Sci*, 2002, **37**(17), p 3623–3630 in English
26. M. Erdogan and R. Priestner, Effect of Epitaxial Ferrite on Yielding and Plastic Flow in Dual Phase Steel in Tension and Compression, *Mat. Sci. Tech.*, 1999, **15**(11), p 1273–1284 in English
27. M. Erdogan and R. Priestner, Effect of Martensite Content, its Dispersion, and Epitaxial Ferrite Content on Bauschinger Behaviour of Dual Phase Steel, *Mat. Sci Tech.*, 2002, **18**(4), p 369–376 in English
28. M. Erdogan, Effect of Austenite Dispersion on Phase Transformation in Dual Phase Steel, *Scrip. Mat.*, 2003, **48**(5), p 501–506 in English
29. V. Franetovic, M.M. Shea, and E.F. Ryntz, Transmission Electron Microscopy Study of Austempered Nodular Iron: Influence of Silicon Content, Austenitizing Time and Austempering Temperature, *Mater. Sci. Eng.*, 1987, **96**, p 231–245 in English
30. J.L. Garin and R.L. Mannheim, Strain-induced Martensite in ADI Alloys, *J. Mater. Proc. Tech.*, 2003, **143–144**, p 347–351 in English
31. W.S. Zhou, Q.D. Zhou, and S.K. Meng, Lubricated Sliding and Rolling Wear of Austempered Ductile Iron, *Wear*, 1993, **162–164**(2), p 696–702 in English
32. P. Mayr, H. Vetters, and J. Walla, Investigations on the Stress Induced Martensite Formation in Austempered Ductile Cast Iron (ADI), *Proc. 2nd Int. Conf. on Austempered Ductile Cast Iron*, Geared Research Institute, 1986 (Ann Arbor), p 171–178
33. J.J. Vuorinen, Strain Hardening Mechanism and Characteristics of Austempered Ductile Iron, *AFS Trans.*, 1986, **94**, p 577–588 in English
34. W.R. Cribb and J.M. Rigsbee, Work-Hardening Behavior and its Relationship to the Microstructure and Mechanical Properties of Dual-Phase Steels, *Structure and Properties of Dual-Phase Steel*, R.A. Kot and J.W. Morris, Ed., AIME, 1979 (New York), p 91–117
35. D.K. Matlock, G. Krauss, L.F. Ramos, and G.S. Huppi, A Correlation of Processing Variables with Deformation of Dual-Phase Steels, *Structure and Properties of Dual Phase Steels*, R.A. Kot and J.W. Morris, Ed., AIME, 1979 (New York), p 62–89